Ferroelectrics, 334:135–145, 2006

ISSN: 0015-0193 print / 1563-5112 online
DOI: 10.1080/00150190600692823

Taylor & Francis
Taylor & Francis Group

Crystal Structure and Ferroelectric Properties of SBT Doped with Praseodymium

J. MATA,[1,*] A. DURÁN,[1] E. MARTÍNEZ,[1] R. ESCAMILLA,[2] J. HEIRAS,[1] AND J. M. SIQUEIROS[1]

[1]Centro de Ciencias de la Materia Condensada, UNAM, Apdo. Postal 2681, C. P. 22800, Ensenada, B. C., México
[2]Instituto de Investigaciones en Materiales, UNAM, México, D. F., 04510, México

The $Sr_{1-x}Pr_xBi_2Ta_2O_9$ ferroelectric ceramic system whit Praseodymium concentration between 0 and 0.20 was studied. DRX show that the Pr-ion substitutes the Sr-ion in the main structure and, as a consequence the unit cell volume decreases monotonically. Thermoelectric Analysis and ferroelectric hysteresis measurements were performed. From the ε-T curves it was observed that the transition temperature depends almost linearly on Pr content. Broad phase transitions were also observed, a typical behavior of ferroelectric materials with diffuse phase transition. The diffuseness coefficient increases with Pr content according to the Isupov model, due to higher cationic disorder in the structure.

Keywords SBT polycrystals; rare earth doping; phase transition

I. Introduction

$SrBi_2Ta_2O_9$ (SBT) is a ferroelectric material that has attracted much interest as an unleaded alternative for PZT in ferroelectric non-volatile memory devices (*FeRAM*). SBT presents very good fatigue endurance, lower switching voltages and small polarization values [1, 2]. The ferroelectricity in SBT was discovered at the beginning of the 1960s [3, 4]. In the structure of SBT, two layers of TaO_6 octahedra in the $SrTa_2O_7$ perovskite blocks are sandwiched between bismuth oxide layers (Bi_2O_2), and Sr occupies the cavity between the octahedra [5, 6].

It has been demonstrated by Noguchi et al. that rare earth (RE) cations of La, Ce, Pr, Nd and Sm as well as Bi are substituted at the *A* site with Sr vacancies modifying substantially the SBT properties; they have also showed that praseodymium ions are substituted at the Sr site as Pr^{+3} and that Sr vacancies are created for compensating the charge difference between Sr^{+2} and Pr^{+3}.

Noguchi et al. have reported that La−, Nd−, and Sm–SBT ($x = 0.2$) show a large remanent polarization (*Pr*) compared with SBT in spite of having a smaller spontaneous polarization [7, 8].

Paper originally presented at IMF-11, Iguassu Falls, Brazil, September 5–9, 2005; received for publication January 26, 2006.
*Corresponding author. E-mail: jmata@ccmc.unam.mx

Recently, other authors [9–10] have reported that $Sr_{1-x}Pr_xBi_2Ta_2O_9$ SBT (SBT-Pr) ceramics exhibit a large remnant polarization and low coercitive field. In this structure, it is proposed the Pr^{3+} ions substitute the Sr sites with the presence of strontium vacancies to maintain the charge neutrality [8]. While bismuth oxide layers are hard to modify, the perovskite blocks accommodate a large variety of cations, as well as Curie temperature (T_C) changes in a wide temperature range [11, 12]. Although SBT-Pr system has been studied very recently, its dielectric properties for the low Pr content ($x < 0.2$) are still not studied. The purpose of this work is the study of the crystal structure and the determination, with high precision, of the composition and chemical occupancies of the three Pr, Sr and Bi crystallographic sites using the Rietveld refinement technique. Also, to analyze the nature of the phase transition and to study the influence of the praseodymium content on the crystal and ferroelectric properties of the system for low Pr concentrations. The analysis of the nature of the phase transition through the Isupov's model and a detailed study of the behavior of the system as a function of composition is done for the first time.

II. Experimental

Ceramic samples of $Sr_{1-x}Pr_xBi_2Ta_2O_9$ (SBT-Pr) with $x = 0$, 0.01, 0.05, 0.10, 0.15 and 0.20 were synthesized by solid-state reaction. Starting materials of $SrCO_3$ (99,9%), $BaCO_3$ (99,9%), Bi_2O_3 (99,9%), Ta_2O_5 (99,9%) and Pr_6O_{11} (99,9%) were mixed in stoichiometric proportions by ball milling. The resulting powder was calcined at 900°C for 5 hours, subsequently pressed into 1 cm diameter discs, placed in a crucible under a Bi_2O_3 controlled atmosphere and sealed with powdered alumina and finally sintered at 1250°C for 2 h.

Phase identification in the samples was carried out with a Siemens D5000 X-ray diffractometer using Cu-K_α radiation and Ni filter. Intensities were measured in steps of 0.02° for 10 seconds in the 2θ range of 5° to 120° at room temperature. The crystallographic phases were identified by comparison with the X-ray patterns of the JCPDS database. Crystallographic and structural parameters were refined by the Rietveld method using the QUANTO program [12–14] with multi-phase capability based on $A2_1am$ orthorhombic symmetry.

Ag electrodes were placed on the discs of the polished ceramic samples. Capacitance measurements were carried out from room temperature up to 450°C in the frequency range of 10 kHz–1 MHz using an LCR bridge (HP-4284A) working at ten different frequencies. The hysteresis loop measurements were performed using an RT66A ferroelectric tester by Radiant Technologies Inc. at room temperature.

III. Results and Discussion

X-Ray Diffraction

The measured density calculated according to the dimensions of the SBT-Pr samples, sintered at 1250°C, was 95% of the theoretical density. X-ray diffraction patterns show that the samples are essentially single phase. Figure 1 shows X-ray diffraction patterns for $(Sr_{1-x}Pr_x)Bi_2Ta_2O_9$, with $x = 0 \leq x \leq 0.2$ samples. The structural analysis based on $A2_1am$ orthorhombic symmetry indicates that all samples correspond to the $SrBi_2Ta_2O_9$ structure. In the refinement process, the substitution of Pr ions in Sr sites was taken into account. Figure 2 shows, as example, a fitted pattern for the $x = 0.05$ sample. Detailed results of the structural refinement are listed in Table 1. The first three rows show the trend of the lattice parameters at room temperature with the increase in Pr content. For $x = 0$,

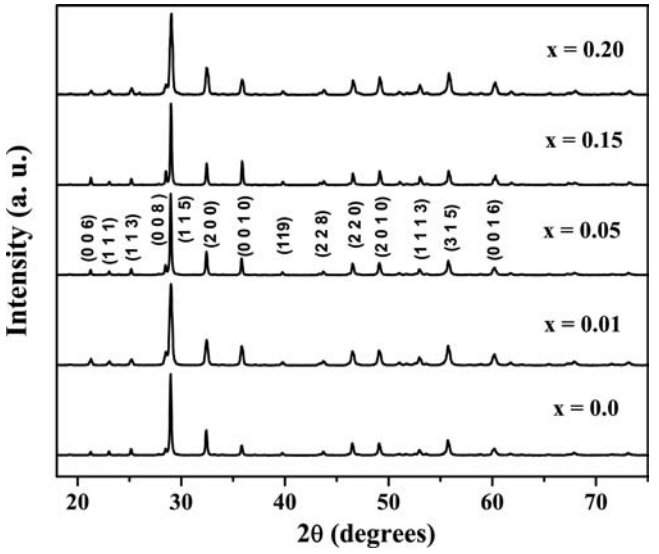

Figure 1. X-ray diffraction patterns for the $Sr_{1-x}Pr_xBi_2Ta_2O_9$ samples.

the lattice parameters are a = 5.5195(3) Å, b = 5.5170(4) Å and c = 25.052(2) Å which are in good agreement with the reported data for SBT [14]. The atomic position, refined according to the crystal symmetry, also agree well with published results [11,14]. It is observed that as x is increased from x = 0 to 0.15 of Pr-ion, the a, b and c lattice parameters decrease as can be clearly seen in Fig. 3. As a consequence of those changes, the unit-cell volume decreases and the orthorhombic distortion (b/a) increases from 0.9995 to 1.0012. However, an unexpected change in the unit cell parameters is observed for the x = 0.2 sample (see Fig. 3). The shrinkage of the unit cell may be explained considering the ionic

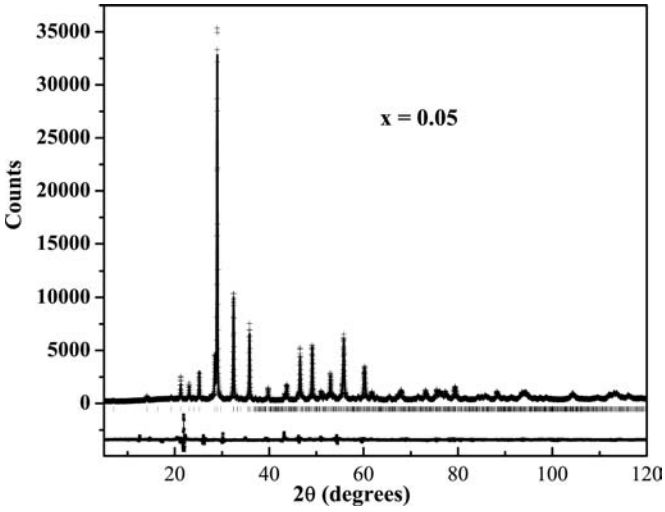

Figure 2. Rietveld refinement of the XRD pattern for the x = 0.05 sample. Experimental spectrum (+), calculated pattern (continuous line), calculated peaks positions (|), and difference (dots).

Table 1
Structural parameters obtained for Rietveld refinement for the $Sr_{1-x}Pr_xBi_2Ta_2O_9$ for $0 \leq x \leq 0.20$ at 295 K.

	x =	0.0	0.01	0.05	0.15	0.2
	a (Å)	5.5195 (3)	5.5195 (2)	5.5105 (2)	5.5086 (4)	5.5169 (4)
	b (Å)	5.5170 (4)	5.5170 (3)	5.5171 (3)	5.5152 (2)	5.5081 (3)
	c (Å)	25.052 (2)	25.052 (2)	25.037 (3)	25.004 (4)	25.035 (4)
	b/a	0.9995	0.9995	1.0001	1.0012	0.9984
	V ($Å^3$)	762.86	762.90	760.41	759.64	760.75
Bi	x	0.4634 (2)	0.4638 (2)	0.4645 (3)	0.4663 (5)	0.4634 (3)
Sr	y	0.7764 (1)	0.7763 (1)	0.7759 (2)	0.7750 (2)	0.7764 (3)
	z	0.1999 (2)	0.1999 (2)	0.1999 (1)	0.200 (1)	0.1999 (2)
Ta	B ($Å^2$)	1.13 (3)	1.08 (3)	0.91 (4)	0.98 (4)	1.02 (4)
	y	0.2567 (3)	0.2566 (4)	0.2561 (2)	0.2550 (2)	0.2567 (2)
	B ($Å^2$)	0.7 (1)	0.7 (1)	0.19 (1)	0.11 (2)	0.13 (1)
	x	0.5104 (2)	0.5104 (3)	0.5105 (4)	0.5106 (5)	0.5104 (3)
O (1)	y	0.7480 (2)	0.7480 (2)	0.7480 (3)	0.7479 (3)	0.7480 (3)
	z	0.4148 (4)	0.4148 (3)	0.4149 (3)	0.4150 (2)	0.4148 (1)
	B ($Å^2$)	0.05 (3)	0.11 (3)	0.21 (4)	0.20 (4)	0.08 (4)
O (2)	x	0.5248 (2)	0.5247 (2)	0.5243 (1)	0.5234 (2)	0.5248 (2)
	y	0.2892 (4)	0.2893 (3)	0.2898 (4)	0.2911 (4)	0.2892 (4)
	B ($Å^2$)	1.7 (9)	2.4 (9)	0.81 (3)	1.2 (7)	0.87 (1)
	x	0.5219 (4)	0.5219 (4)	0.5217 (4)	0.5212 (4)	0.5219 (3)
O (3)	y	0.6990 (2)	0.6989 (4)	0.6985 (3)	0.6974 (4)	0.6990 (4)
	z	0.3418 (3)	0.3418 (3)	0.3418 (2)	0.3418 (3)	0.3419 (5)
	B ($Å^2$)	0.6 (5)	1.4 (6)	2.9 (7)	3.0 (1)	0.63 (3)
	x	0.7381 (2)	0.7381 (1)	0.7382 (2)	0.7385 (1)	0.7381 (2)
O (4)	y	0.9923 (2)	0.9923 (2)	0.9923 (4)	0.9924 (4)	0.9923 (4)
	z	0.2507 (1)	0.2507 (1)	0.2508 (3)	0.2507 (3)	0.2508 (3)
	B ($Å^2$)	4.4 (7)	3.1 (7)	4.7 (8)	4.0 (2)	1.29 (6)
	x	0.7554 (3)	0.7553 (3)	0.7549 (2)	0.7538 (3)	0.7554 (3)
O (5)	y	0.9867 (2)	0.9866 (3)	0.9865 (4)	0.986082)	0.9867 (2)
	z	0.0696 (2)	0.0696 (2)	0.0696 (2)	0.0695 (1)	0.0696 (2)
	B ($Å^2$)	0.7 (4)	0.7 (7)	0.6 (2)	0.8 (1)	0.78 (2)
	x	0.7909 (3)	0.7908 (4)	0.7905 (3)	0.7898 (2)	0.7909 (3)
	y	0.9807 (2)	0.9806 (2)	0.9804 (2)	0.9799 (2)	0.9807 (1)
	z	0.5836 (2)	0.5835 (1)	0.5835 (1)	0.5835 (1)	0.5836 (3)
	B ($Å^2$)	0.8 (8)	0.7 (7)	0.8 (6)	1.1 (7)	1.4 (1)
	R_p (%)	9.8	9.9	6.4	7.7	10.2
	R_{wp} (%)	12.5	12.6	10.8	13.6	13.1
	R_{exp} (%)	7.0	7.1	3.8	3.9	8.6
	χ^2 (%)	1.7	1.8	2.8	3.4	1.5

Note. Space group: $A\,2_1a\,m$. Atomic positions: Bi: 8b (x, y, z); Sr: 4a (0, y, 0); Ta: 8b (x, y, z); O(1): 4a (x, y, 0); O(2): 8b (x, y, z), O(3): 8b (x, y, z), O(4): 8b (x, y, z) and O(5): 8b (x, y, z).

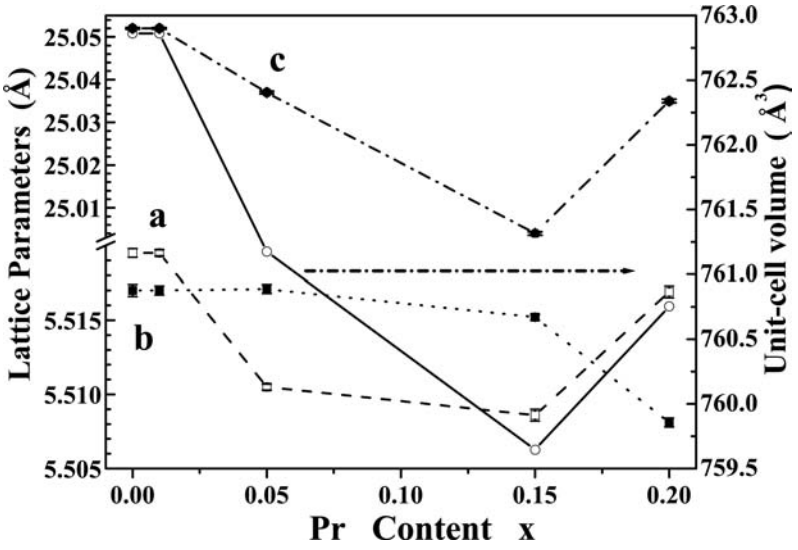

Figure 3. Crystal lattice parameters (a, b, c) and unit cell volume as functions of Pr-ion content (x) for $Sr_{1-x}Pr_xBi_2Ti_2O_9$.

radii of the Sr^{2+}, Pr^{3+} and Pr^{4+} ions. Recent studies of x-ray photoelectron spectroscopy (XPS) in SBT:Pr and $Sr_{1-x}Pr_xTiO_3$ (STO:Pr) showed that the Pr ion is substituted in the Sr site as a mixed valence of Pr^{3+}/Pr^{4+} with a molar ratio of 2:1 [7, 15]. Thus, it is noted that the ionic radii of the Sr^{2+} ion with twelve coordination number is 1.44 Å while that of the Pr^{3+} and Pr^{4+} ions in eight coordination number are 1.179 Å and 0.96 Å, respectively [17]. From these values, it is clear that the decrease of the unit cell volume can be related to the substitution of Pr^{4+} and/or Pr^{3+} ions into the Sr^{2+} sites. On the other hand, the unexpected change of the refined parameters for $x = 0.2$ is not yet understood in detail but it may be due to the presence of an intermediate phase in SBT induced by Pr doping. This assumption is consistent with the fact that the $A2_1am$ space group is not an isotropy subgroup of the tetragonal *I4/mmm*. On the other hand, several polar space groups such as *Fmmm*, *Amam*, *Aba2*, *I42m* have been proposed [17] which can be induced by the local environment of the doping cation. Hence, a future comparison with related Aurivillius phases with more sensitive diffraction experiments is planed for $x \geq 0.2$ samples.

To elucidate whether the Pr ion really substitutes at the Sr rather than the Bi site, the Rietveld refinement analyses revealed the following facts. First, there is a decrease of the distortion in the TaO_6 octahedra, defined as octahedral distortion (Δ_{oct}) in Table 2, which changes from 3.72 to 3.51 for $0 \leq x \leq 0.15$. Second, the buckling of the TaO_6 octahedral increasing along the b-axis with tilting angle varying from 6.43 to 6.67° with respect to the c-axis (obtained from the Ta-O(1)-Ta bond angle, see Table 2) and finally, an increase of the thermal parameter (B) in the Sr site from 0,7 to ∼1,5 it is noted as well as a slight decrease in the Bi site (see Table 1). These results strongly suggest that the Pr ion is substituted principally in the Sr site with a smaller ionic radius and likely producing cation vacancies in this site, since a large B parameter is frequently correlated with the vacancies. Recently, Neutron diffraction studies in Sr-deficient SBT [10] revealed a large B parameter in the Sr site with respect to the stoichiometric one suggesting the presence of vacancies in this site.

Additionally, it is observed a large thermal parameter in the apical oxygen O(2) of the octahedron, as Pr ion concentration is increased,. This result also suggests the formation of

Table 2
Bond lengths (Å) and bond angles (°) for TiO_6 octahedra in the $Sr_{1-x}Pr_xBi_2Ta_2O_9$ at 295 K.

x =	0.0	0.01	0.05	0.15	0.2
Ta-O(1)	2.148 (2)	2.148 (2)	2.145 (3)	2.140 (2)	2.147 (3)
Ta-O (2)	1.847 (3)	1.850 (2)	1.850 (3)	1.851 (3)	1.846 (2)
Ta-O (4)	1.952 (2)	1.952 (3)	1.951 (3)	1.953 (3)	1.950 (3)
Ta-O (4)	2.015 (3)	2.015 (1)	2.011 (2)	2.008 (3)	2.013 (2)
Ta-O (5)	1.926 (1)	1.927 (2)	1.928 (2)	1.932 (2)	1.924 (2)
Ta-O (5)	2.012 (2)	2.011 (3)	2.007 (2)	2.001 (3)	2.010 (1)
$\langle$Ta-O$\rangle_{average}$	1.989	1.984	1.982	1.981	1.982
Octahedral distortion (Δ_{oct})	3.72	3.64	3.59	3.51	3.68
	Main and tilting angles of the TiO_6 octhaedral				
O(4)-Ta-O(4)	88.31 (2)	88.31 (3)	89.24 (2)	88.27 (2)	88.37 (2)
O(5)-Ta-O(5)	89.30 (2)	89.30 (3)	88.22 (2)	89.24 (1)	89.36 (3)
O(4)-Ta-O(5)	93.30 (1)	93.27 (2)	93.29 (1)	93.06 (2)	93.25 (2)
O(4)-Ta-O(5)	86.33 (2)	86.35 (1)	86.54 (2)	86.76 (3)	86.28 (1)
Ta-O(1)-Ta	167.13 (2)	167.11 (2)	167.00 (3)	166.66 (2)	167.14 (3)
Tilting angle (α)	6.43	6.44	6.5	6.67	6.43

Note. The octahedral distortion is defined as $\Delta_{oct} = 10 \times (\Sigma(\text{M-O}_i) - \langle\text{M-O}\rangle_{average})/\langle\text{M-O}\rangle_{average}$ [14].

oxygen vacancies and, as a consequence the decrease of the octahedral distortion mentioned above. Regardless of this facts, the progressive introduction of Pr ion in the lattice give rise to notable changes in the ferroelectric properties as is explained in the next part.

Dielectric Behavior

From the analysis of the results it was observed that the dielectric properties as well as the transition temperature strongly depend on Pr content. Figure 4 shows the dependence of the permittivity (ε) with temperature, measured at 1 kHz for the five studied compositions. The permittivity curves show: a) a decrease in the transition temperature with increasing Pr content and b) broad phase transitions indicating a diffuse phase transition (DPT) attributable to the existence of polar microregions above the nominal transition temperature mainly as a consequence of composition and local polarization fluctuations. In Fig. 4 it is also observed that the transition temperature (T_m) decreases almost linearly with Pr content. The linear behavior of T_m with Pr concentration leads to the conclusion that praseodymium is incorporated in the perovskite structure of the SBT system, forming monophasic solid solutions in accordance with XRD observations. An analysis of this type of transition is undertaken in the following section.

Characterization of the ε Peak on the High Temperature Side

A modified Curie-Weiss law is often used to describe the diffuseness of the phase transition:

$$\frac{1}{\varepsilon} - \frac{1}{\varepsilon_{max}} = \frac{(T - T_c)^{\gamma}}{2 \cdot \delta^2 \cdot \varepsilon_{max}} \tag{1}$$

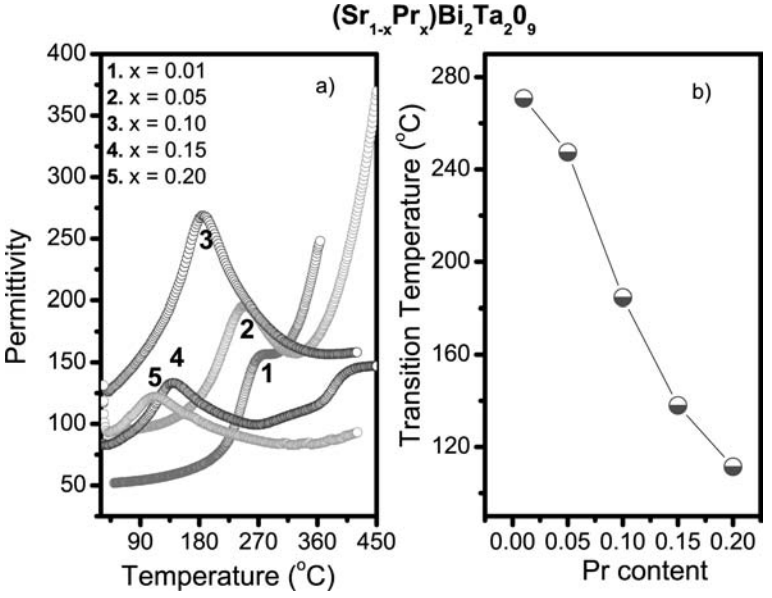

Figure 4. a) Temperature dependence of $\varepsilon/\varepsilon_o$ at 1 kHz in $Sr_{1-x}Pr_xBi_2Ta_2O_9$ polycrystals. b) Praseodymium content dependence of the transition temperature. (See Color Plate VIII)

where γ is assumed to be constant. The limiting values $\gamma = 1$ and $\gamma = 2$ reduce the expression to the Curie-Weiss law valid for the case of a normal ferroelectric and to the quadratic dependence valid for an ideal diffusive ferroelectric, respectively. Figure 5a shows the inverse of the permittivity as a function of temperature at 1 kHz and the fits to the experimental data using Curie-Weiss law ($\gamma = 1$). In these curves, three different regions may be distinguished: the ferroelectric state at temperatures below the temperature of maximum permittivity (T_m), the state where polar (micro/nano) clusters exist for temperatures between T_m and T_{cw}; and the paraelectric state for temperatures above T_{cw}. The "real" Curie temperature is obtained by the intersection of the linear extrapolation of the curve from the paraelectric state, where the Curie-Weiss law holds, with the temperature axis. T_m would then be the transition temperature of the material should it have a normal order transition instead of a phase transition with polar nanoclusters. In Fig. 5b Ln $(1/\varepsilon - 1/\varepsilon_m)$ vs. Ln $(T - T_m)$ is plotted to show that the Curie-Weiss law does not hold and is not representative of the overall behavior of the material. The regions where the Isupov law ($\gamma = 2$) is valid, allow us to determine the disorder parameter (δ) using Eq. (1) plotting $(1/\varepsilon - 1/\varepsilon_m)$ against $(T - T_m)^2$ for all compositions (see Fig. 6a). The values for δ are reported in the same graph, where an increase in its value is observed with the increase in Pr content. This behavior is explained by the higher disorder associated to the random location of the ions in the crystal sites when $Pr^{+3,+4}$ substitutes Sr^{+2}. The composition fluctuations will then be larger, originating a wider transition temperature distribution.

Ferroelectric Properties

Figure 6b shows the ferroelectric hysteresis loops at room temperature for the studied compositions under a 20 kV/cm applied electric field. The ferroelectric state for each composition at room temperature is proven, although the ferroelectric properties are not better

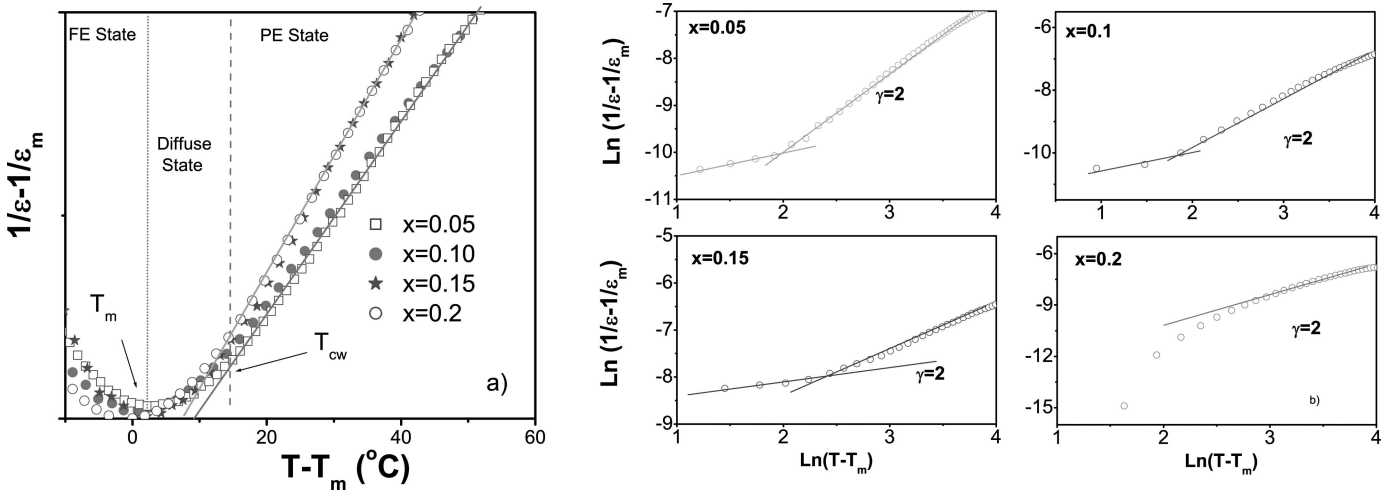

Figure 5. a) The inverse dielectric constant ($1/\varepsilon - 1/\varepsilon_m$) as a function of temperature at 1 kHz for x = 0.05, 0.1, 0.15 and 0.2 in praseodymium content. The line represents the fit using the Curie-Weiss law. b) Ln ($1/\varepsilon - 1/\varepsilon_m$) as a function of Ln ($T - T_m$) for SBT-Pr ceramics. (See Color Plate IX)

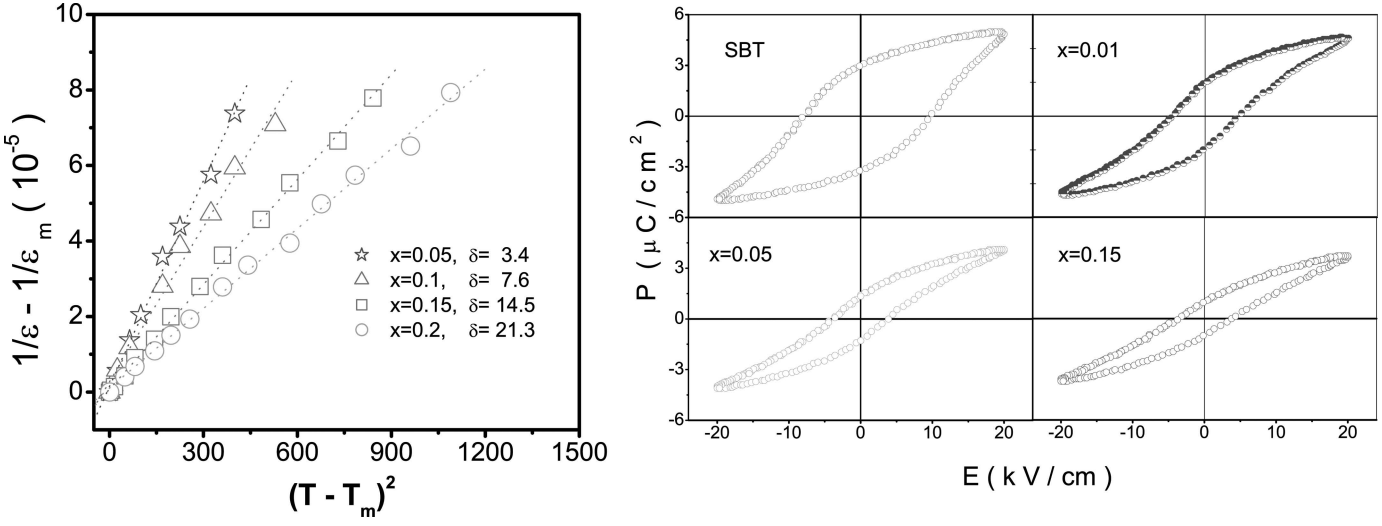

Figure 6. a) $(1/\varepsilon - 1/\varepsilon_m)$ against $(T - T_m)^2$ for all samples. In each case the diffusivity coefficient may be determined through the slope of the respective curve and by using Eq. (1). b) Variations of the hysteresis loop with temperature measured at 20 kV/cm for x = 0.0, 0.01, 0.05 and 0.15 in praseodymium content. (See Color Plate X)

than those of pure SBT. The inclusion of praseodymium in low concentrations lowers the remanent polarization of SBT in contrast to the results reported by Noguchi for x = 0.2 [7–9].

It is observed that polarization values decrease with the increase of Pr content. Space charge and ionic defects such as strontium vacancies are likely to assemble in the vicinity of charged domain walls and form a dipolar defect complex that promotes domain pinning suppressing the ferroelectric behavior.

IV. Conclusions

The electrical and structural properties of the monophasic SBT-Pr ceramic system with different concentration of Pr-ion were studied. The permittivity curves show broad phase transitions, typical of ferroelectrics with diffuse phase transition. X-ray diffraction patterns show that the samples are essentially single phase. The transition temperature and remnant polarization decrease linearly with increasing Pr content consistent with the lowering of the maximum permittivity. The analysis of the nature of the phase transition through Isupov's model reveals a high cationic disorder in the structure. An increase of the disorder is found with the rise of Pr content, reaffirming that its inclusion enhances the structural disorder, increasing therefore the diffuse character of the transition, resulting in the loss of the long-range ferroelectric ordering. The hysteresis loop indicates that the substitution of Sr^{2+} by Pr^{3+} in small concentration lowers the polarization due possibly to strong domain pinning mechanisms induced by the ionic defects. Furthermore, it is observed that polarization values decrease with the increase of the Pr content up to x = 0.15 disagreeing with the results of other authors for x = 0.2 [7–9]. Research to establish the difference between the high and low Pr content is in progress.

Aknowledgments

The authors would like to thank Pedro Casillas, M. Sainz, J. Peralta and E. Aparicio (CCMC-UNAM) for their technical assistance. This work is partially supported by CONACyT México, projects 47714-F and 40604-F and DGAPA-UNAM projects IN116703 and IN100903.

References

1. J. F. Scott and C. A. Araujo, Ferroelectric Memories. *Science* **246**, 1400–1405 (1989)
2. C. A. Paz de Araujo, J. D. Cuchiaro, L. D. McMillan, M. C. Scott, and J. F. Scott, Fatigue-free ferroelectric capacitors with platinum electrodes. *Nature* **374**, 627–629 (1995).
3. E. C. Subbarao, Family of ferroelectric bismuth compounds. *J. Phys. Chem. Solids* **23**, 665–676 (1962).
4. E. C. Subbarao, *J. Am. Ceram. Soc.* **45**, 166 (1962).
5. Y. Shimakawa, Y. Kubo, Y. Nakagawa, S. Goto, T. Kamiyama, H. Asano, and F. Izumi, Crystal structure and ferroelectric properties of $ABi_2Ta_2O_9$ (A=Ca, Sr, and Ba). *Phys. Rev.* **B61**, 6559–6564 (2000).
6. Y. Noguchi, A. Kitamura, L. C. Woo, M. Miyayama, K. Oikawa, and T. Kamiyama, Praseodymium-modified $SrBi_2Ta_2O_9$ with improved polarization properties at low electric field. *J. Appl. Phys.* **94**, 6749–6752 (2003).
7. Y. Noguchi, M. Miyayama, K. Oikawa, T. Kamiyama, M. Osada, and M. Kakihana, Defect Engineering for Control of Polarization Properties in $SrBi_2Ta_2O_9$. *Jpn. J. Appl. Phys.* **41**, 7062–7075 (2002).

8. A. Kitamura, Y. Noguchi, and M. Miyayama, Polarization properties of praseodymium-modified $SrBi_2Ta_2O_9$ ceramics and thin films prepared by sol–gel method. *Materials Letters* **58**, 1815–1818 (2004).
9. J. S. Kim, C. Cheon, H. S. Shim, and C. H. Lees, Crystal structure and phase transitions of $Sr_{1\pm x}Bi_{2\pm y}Ta_2O_9$ ceramics. *J. Eur. Ceram. Soc.* **21**, 1295–1298 (2001).
10. Y. Shimakawa, Y. Kubo, Y. Nakagawa, T. Kamiyama, H. Asano, and F. Izumi, Crystal structures and ferroelectric properties of $SrBi_2Ta_2O_9$ and $Sr_{0.8}Bi_{2.2}Ta_2O_9$. *Appl. Phys. Lett.* **74**, 1904–1906 (1999).
11. S. Kamba, J. Pokorný, V. Porokhonskyy, J. Petzelt, M. P. Moret, A. Garg, Z. H. Barber, and R. Zallen, Ferroelastic phase in $SrBi_2Ta_2O_9$ and study of the ferroelectric phase transition dynamics. *Appl. Phys. Lett.* **81**, 1056–1058 (2002).
12. A. S. Wills and I. D. Brown, QUANTO (*A Rietveld program for quantitative phase analysis of polycrystalline mixtures*) VaList, CEA, France (1999).
13. Y. Noguchi, M. Miyayama, and T. Kudo, Direct evidence of *A*-site-deficient strontium bismuth tantalate and its enhanced ferroelectric properties. *Phys. Rev.* **B63**, 214102-214102-5 (2001).
14. A. D. Rae, J. G. Thompson, and R. L. Withers, Structure refinement of commensurately modulated bismuth strontium tantalate, $Bi_2SrTa_2O_9$. *Acta Cryst.* **B48**, 418–428 (1992).
15. A. Durán, E. Martínez, J. A. Díaz, and J. Siqueiros, Ferroelectricity at room temperature in Pr-doped $SrTiO_3$. *J. Appl. Phys.* **97**, 104109-104109-4 (2005).
16. R. D. Shannon, Revised effective ionic radii and systematic studies of interatomic distances in halides and chalcogenides. *Acta Cryst.* **A32**, 751–767 (1976).
17. J. M. Pérez-Mato, M. Arroyo, A. Garcia, P. Blaha, K. Schwarz, J. Schweifer, and K. Parlinki, Competing structural instabilities in the ferroelectric Aurivillius compound $SrBi_2Ta_2O_9$. *Phys. Rev.* **B70**, 214111-214111-14 (2004).
18. V. V. Kirillov and V. A. Isupov, Relaxation polarization of Pb $Mg_{1/3}Nb_{2/3}O_3$ (PMN)-A ferroelectric with a diffused phase transition. *Ferroelectrics* **5**, 3–9 (1973).